ARTICLES

Real-time tRNA transit on single translating ribosomes at codon resolution

Sotaro Uemura[1,2], Colin Echeverría Aitken[1,3]†, Jonas Korlach[4], Benjamin A. Flusberg[4], Stephen W. Turner[4] & Joseph D. Puglisi[1,3]

Translation by the ribosome occurs by a complex mechanism involving the coordinated interaction of multiple nucleic acid and protein ligands. Here we use zero-mode waveguides (ZMWs) and sophisticated detection instrumentation to allow real-time observation of translation at physiologically relevant micromolar ligand concentrations. Translation at each codon is monitored by stable binding of transfer RNAs (tRNAs)—labelled with distinct fluorophores—to translating ribosomes, which allows direct detection of the identity of tRNA molecules bound to the ribosome and therefore the underlying messenger RNA (mRNA) sequence. We observe the transit of tRNAs on single translating ribosomes and determine the number of tRNA molecules simultaneously bound to the ribosome, at each codon of an mRNA molecule. Our results show that ribosomes are only briefly occupied by two tRNA molecules and that release of deacylated tRNA from the exit (E) site is uncoupled from binding of aminoacyl-tRNA site (A-site) tRNA and occurs rapidly after translocation. The methods outlined here have broad application to the study of mRNA sequences, and the mechanism and regulation of translation.

During translation, the ribosome progressively coordinates the dynamic interplay of tRNA and protein factors to decipher individual codons of an mRNA molecule and synthesize protein. The ribosome contains three tRNA-binding sites corresponding to three adjacent codons[1]. As it elongates, the ribosome repetitively selects aminoacylated tRNA molecules at the A site, orienting them for peptide-bond formation with peptidyl tRNA positioned in the P site. Peptidyl transfer is followed by the coordinated movement of the A- and P-site tRNAs into the P and E sites, respectively, thus preparing the deacylated tRNA for dissociation from the ribosome. During this translocation step, which is catalysed by the GTPase EF-G, the ribosome simultaneously steps along the mRNA, positioning the next codon in the A site and preparing to select another aminoacylated tRNA.

Although dynamic changes in ligand occupancy and positioning in the A, P and E sites are intimately tied to the mechanism of translation[2–5], the timing and relation of aminoacylated tRNA arrival at the A site, as a ternary complex with EF-Tu•GTP, and dissociation of deacylated tRNA from the E site remain unknown. Single-molecule fluorescence methods have recently probed dynamics during translation, such as the selection of tRNA during elongation and ribosomal conformational changes (reviewed in ref. 6). However, traditional single-molecule fluorescence only allows observation of fluorescent ligands in the nanomolar range, well below the physiological micromolar concentration of most components of the translational apparatus.

Real-time translation in ZMWs

ZMWs (Fig. 1a) are nanophotonic confinement structures consisting of circular holes of diameter 50–200 nm in a metal cladding film deposited on a solid, transparent substrate[7]. In conjunction with laser-excited fluorescence, ZMWs provide observation volumes on the order of zeptolitres (10^{-21} l), three to four orders of magnitude smaller than far-field excitation volumes. This drastically reduces the background signal from freely diffusing fluorescent molecules, allowing the observation of fluorescent ligands in the micromolar range. Advances in fabrication[8], surface chemistry[9] and detection instrumentation[10] have allowed direct monitoring of DNA polymerization in ZMWs[11]. The binding of labelled ligands to an enzyme immobilized in a ZMW is detected as pulses of fluorescent light. Here we adapt this instrumentation to the study of translation. Using ZMWs, we observe real-time selection and transit of fluorescently labelled tRNAs at micromolar concentrations (Fig. 1b) on single ribosomes during multiple rounds of translation elongation.

Binding of tRNA on single ribosomes was tracked using tRNAs that were specifically dye-labelled at their elbow positions without affecting their function[12,13]. Ribosomes were immobilized in ZMWs as 70S initiation complexes—containing fMet-(Cy3)tRNA^{fMet}—assembled on biotinylated mRNAs, which were tethered to the biotin–polyethylene glycol (PEG)-derivatized bottom of ZMWs through neutravidin-biotin linkages; mRNAs contained 5′-UTR (untranslated region) and Shine-Dalgarno sequences from the T4 gene 32, an initiation codon and coding sequence of 3–12 codons, terminated by a stop (UAA) codon followed by four phenylalanine codons (Figs 2a and 3a). Cy3 fluorescence from an immobilized complex confirmed the presence of initiator tRNA and marked a properly assembled and immobilized ribosome in a ZMW. The number of ribosome complexes immobilized per individual ZMW surface increased at higher concentrations of ribosomal complex, obeying Poisson statistics, and, as expected, could be blocked by addition of free biotin (Supplementary Fig. 1). Ellipsometry and ZMW experiments in the absence of ribosomes confirmed minimal non-specific surface adsorption of translational components (100 μM tRNA, 1 μM EF-Tu and EF-G) (Supplementary Fig. 2).

To confirm the use of ZMWs for investigating translation, we used fluorescence resonance energy transfer (FRET)—a sensitive distance

[1]Department of Structural Biology, Stanford University School of Medicine, Stanford, California 94305-5126, USA. [2]Japan Science and Technology Agency, 4-1-8, Honcho, Kawaguchi, Saitama 332-0012, Japan. [3]Biophysics Program, Stanford University School of Medicine, Stanford, California 94305-5126, USA. [4]Pacific Biosciences, Inc., 1505 Adams Drive, Menlo Park, California 94025-1451, USA. †Present address: Department of Biophysics and Biophysical Chemistry, John Hopkins University School of Medicine, 725 N. Wolfe Street, WBSB 713, Baltimore, Maryland 21205-2185, USA.

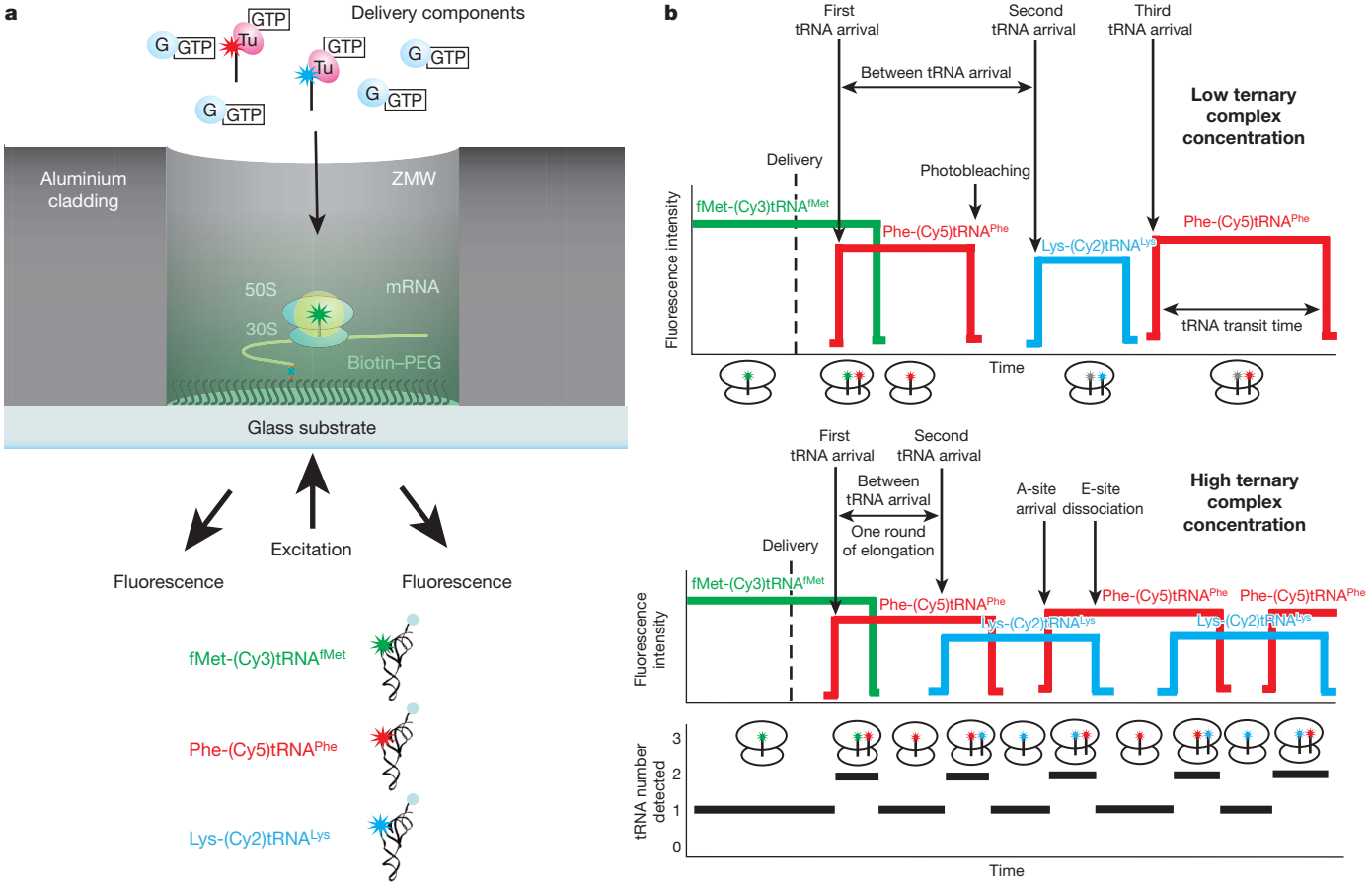

Figure 1 | Translation in ZMWs. a, Experimental setup. ZMWs are cylindrical nanostructures with varying diameters (~50–200 nm). The aluminium side wall and quartz bottom surfaces are derivatized to allow specific biotin–streptavidin interactions on the quartz surface and to block non-specific interactions of molecules with ZMWs[9,11]. Ribosomal complexes are specifically immobilized in the bottom of derivatized ZMWs using biotinylated mRNAs. Ternary complexes Cy5-labelled Phe-tRNA^{Phe}-EF-Tu(GTP) and Cy2-labelled Lys-tRNA^{Lys}-EF-Tu(GTP), along with EF-G(GTP), are delivered to a ZMW surface-immobilized, initial ribosome complex containing Cy3-labelled fMet-tRNA^{fMet}. Fluorescence is excited by illumination at 488, 532 and 642 nm, and Cy2, Cy3 and Cy5 fluorescence are simultaneously detected using previously described instrumentation[10,11]. **b**, Expected signal sequence. Initiation complexes are detected by fluorescence of fMet-(Cy3)tRNA^{fMet} bound at an initiation codon. Fluorescent tRNAs are delivered as ternary complexes. Arrival of Phe-(Cy5)tRNA^{Phe} or Lys-(Cy2)tRNA^{Lys} at the ribosomal A site is marked by a red or blue fluorescent pulse. At low concentrations of ternary complex, tRNA arrival times are slow (much longer than 1 s), and Cy5- or Cy2-labelled tRNAs can photobleach on the ribosome while waiting for translocation. In the absence of photobleaching, the length of a pulse represents the transit time of that tRNA on the ribosome. At high concentrations of ternary complex, tRNA arrival times are fast (much less than 1 s), and fluorescent pulses are overlapped, which indicates simultaneous occupancy by two tRNA molecules. The tRNA occupancy count is shown below the schematic trace.

indicator—to observe the path of incoming A-site tRNA accommodation on the ribosome. We have previously used traditional single-molecule total internal reflection fluorescence (TIRF) to detect FRET between fMet-(Cy3)tRNA^{fMet} in the P site and Phe-(Cy5)tRNA^{Phe} in the A site[12,13]. We repeated these experiments using ZMW-immobilized ribosome complexes and excitation at 532 nm. Using FRET values calibrated in ZMWs, we matched the values and timescales observed in previous tRNA–tRNA FRET experiments at tRNA concentrations up to 600 nM, more than 20-fold higher than previously measured (Supplementary Figs 3 and 4). Consistent with previous single-molecule studies, bimolecular arrival rates of ternary complex to surface-bound ribosomes were decreased by an order of magnitude compared with bulk rates, but unimolecular rates were unaffected. Decreased association rates are likely due to steric and surface effects[14], but ribosomal function is clearly maintained. These results confirmed the functionality of ZMW-immobilized ribosomes and our ability to detect fluorescent tRNA-binding events on individual ribosomes at ternary complex concentrations greater than 100 nM.

Detecting tRNA binding in real time. The basic steps of translation were then observed through direct detection of fluorescently labelled tRNA binding on single ribosomes immobilized in ZMWs. We monitored the binding of ternary complexes Phe-(Cy5)tRNA^{Phe}•EF-Tu•GTP and unlabelled Lys-tRNA^{Lys}•EF-Tu•GTP or labelled Lys-(Cy2)tRNA^{Lys}•EF-Tu•GTP to ribosomes programmed by mRNAs encoding four amino acids (MFFF or MFKF) (Fig. 2a, b); ZMWs were illuminated simultaneously with 488-, 532- and 642-nm excitation. Initiated ribosomes were identified by the presence of fMet-(Cy3)-tRNA^{fMet}; subsequent real-time arrival and occupation of tRNAs on translating ribosomes were detected as fluorescent pulses of appropriate colour[10].

Each tRNA pulse marks the arrival and accommodation of that tRNA within the ribosomal A site. The arrival time of the first elongator tRNA encoded by the mRNA marks the transition of ribosomes into elongation. The time between subsequent tRNA pulse arrivals delineates one round of translational elongation and arrival of tRNA at the next codon (Fig. 1b). This time should depend on the concentration of EF-G, which controls the rate of translocation to the next codon. The duration of each tRNA pulse represents the transit time of that tRNA through the A, P and E sites, followed by dissociation from the ribosome. At the low (<50 nM) factor and tRNA concentrations normally used for single-molecule experiments, photobleaching of ribosome-bound tRNA can also terminate a pulse. Because each pulse describes binding of one tRNA molecule on the ribosome, full

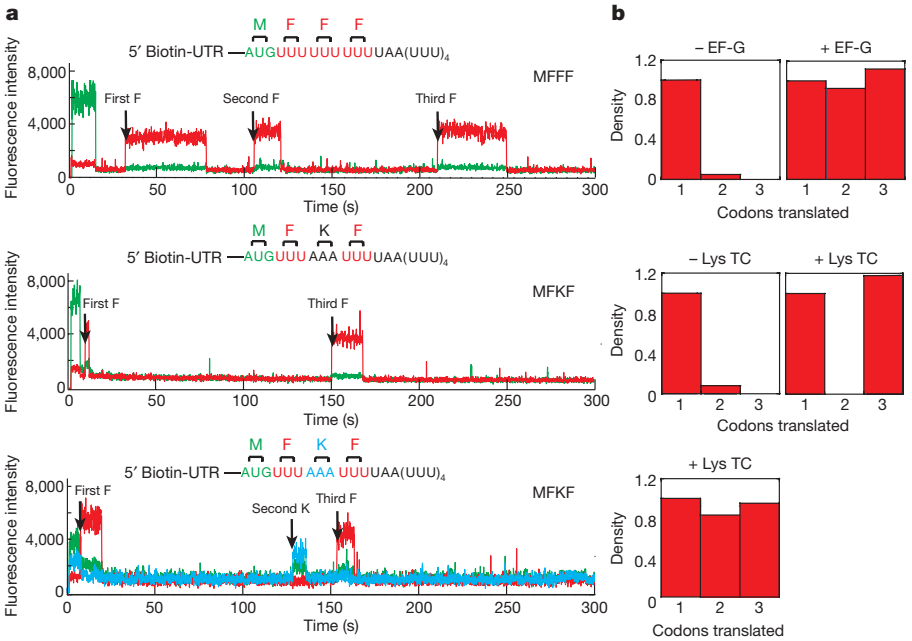

Figure 2 | Monitoring translation by fluorescent tRNA-binding events. **a**, Representative single-ZMW traces of ribosomes translating MFFF mRNA (top) and MFKF mRNA (bottom) in the presence of 30 nM EF-G and 30 nM ternary complex. F, Phe-tRNA^{Phe}; K, Lys-tRNA^{Lys}. **b**, The number of fluorescent pulses observed in ZMWs depends on the presence of EF-G and ternary complex. Event histograms for the three experiments in the absence ($n = 341$) and presence ($n = 304$) of 30 nM EF-G (top), and in the absence ($n = 278$) and presence ($n = 297$) of 30 nM unlabelled Lys-tRNA^{Lys} ternary complex (middle) and presence ($n = 355$) of 30 nM Lys (Cy2)tRNA^{Lys} ternary complex (bottom). Histograms are normalized by the number of ribosomes showing single events.

translation is detected as a series of pulses corresponding to the number and sequential identity of codons in the mRNA.

To define the order and identity of these pulses, initial experiments were performed at concentrations of 30 nM EF-G/30 nM ternary complex, with translation times of about 20 s per codon, which allows P-site tRNAs to photobleach (average lifetime 13.7 s) before the arrival of A-site tRNA. In the absence of EF-G, translation of the MFFF message stalls upon arrival of the first tRNA^{Phe} (Fig. 2b). Cy3 fluorescence is followed only by a single red pulse, indicating binding of a single Phe-(Cy5)tRNA^{Phe} and no subsequent translocation (Fig. 2b). In the presence of 30 nM EF-G, three distinct red fluorescent pulses are observed (Fig. 2a, b). The number of fluorescent tRNA pulses is similarly sensitive to the identity of the A-site codon and the presence of correct ternary complex. Translation of the MFKF mRNA in the presence of EF-G but absence of Lys-tRNA^{Lys} ternary complex results in a single fluorescence pulse following the Cy3 signal, whereas two red pulses are observed upon addition of unlabelled Lys-tRNA^{Lys} ternary complex; finally, two red pulses separated by a blue pulse are observed upon inclusion of fluorescently labelled Lys-(Cy2)tRNA^{Lys} ternary complex. In all traces, brief single-frame (100 ms) bursts in fluorescence can be observed (Fig. 2a). These events were only observed in the presence of 70S ribosomal complexes, and likely represent non-cognate ternary complex sampling at an A-site codon (see below). These results confirm our ability to track translation through sequential stable tRNA-binding events.

Monitoring translation in real time. These tRNA-binding signals were then used to observe full translation of distinct heteropolymeric mRNAs encoding 13 amino acids (M(FK)$_6$ and M(FKK)$_4$). The sequence of the mRNA is readily distinguished from the pattern of fluorescent pulses (Fig. 3a). The number of events observed relates the number of codons translated on each mRNA. At 200-nM ternary complex and 500-nM EF-G, ribosomes translate the entire mRNA (Fig. 3b, red bars). The duration of most tRNA pulses is not limited by photobleaching at these high concentrations, which suggests that the lifetime of each tRNA signal provides a signal for its transit time on the ribosome (see below). Addition of erythromycin, which binds to the exit tunnel of the ribosome[15], blocks translation at six to eight amino acids[16], as expected (Fig. 3b). These data strongly support the direct link between the pattern of tRNA pulses observed in the ZMW and translation.

The arrival of tRNAs at single ribosomes tracks the dynamic composition of the translational apparatus in real time. First tRNA arrival events are fast, as they do not depend on translocation. As predicted, the time between subsequent tRNA arrivals decreases with increasing EF-G concentrations between 30 and 500 nM (Fig. 3c). For codons 2–12, the tRNA transit time is also strongly dependent on EF-G, as it represents at least two rounds of peptide-bond formation and translocation (Fig. 3d). Inhibition of EF-G by fusidic acid, which stabilizes EF-G•GDP on the ribosome after translocation[17], lengthens the transit time by 3.3-fold (Fig. 3d). Arrival of the ribosome at the UGA stop codon after translation of 12 codons leads to a long pulse from the remaining tRNA in the P site of the stalled ribosome. The dwell time for this last tRNA is 4.9-fold longer than for preceding pulses, which emphasizes that photobleaching of the P-site tRNA is not a significant problem using our approach at high-factor concentrations: at 500 nM EF-G, the mean lifetime (4.1 s) of tRNAs bound to the ribosome is significantly shorter than the photobleaching lifetime (17.3 s) observed in experiments at lower concentrations. While paused on the stop codon, tRNA sampling events are observed with short lifetimes (~50 ms for Phe-(Cy5)tRNA^{Phe} or Lys-(Cy2)tRNA^{Lys}) (Fig. 4a, b), which are clearly distinguishable from real tRNA transit events of more than 1 s. These sampling events are consistent with non-cognate ternary-complex interaction[4] with the A site, and their frequency is proportional to ternary-complex concentration (Fig. 4c). All trends discussed above were independent of mRNA sequence.

The total translation time for different mRNAs is characterized by the arrival times of tRNAs at different codons. As expected, translation rates depend on the concentrations of ternary complex and EF-G. For the M(FK)$_6$ mRNA (Fig. 3e), translation rates increased from 0.08 to 0.4 s^{-1} for EF-G concentrations ranging from 30 and 500 nM (200 nM ternary complex). Likewise, increasing the concentration of ternary complex also increased the overall translation rate. At the highest concentrations of ternary complex and EF-G, the translation rate was nearly one codon per second, approaching that obtained using cell extracts *in vitro*[18]. When 30S pre-initiation complexes are immobilized in ZMWs and translation is initiated by addition of 50S subunits, ternary complex and EF-G—requiring initiation before protein synthesis (Supplementary Fig. 5)—the overall translation rate is unaffected, except for a delay (12 s) in arrival of the first tRNA. This delay is consistent with the timescale of 50S subunit joining during initiation[19], before progression to elongation.

Our approach allows analysis of translational rates at each codon of an mRNA molecule. Arrival of the first tRNA is independent of EF-G concentration, as expected. However, the first EF-G catalysed translocation of the ribosome may become the slowest step in elongation, as revealed by the time between arrivals of tRNA molecules

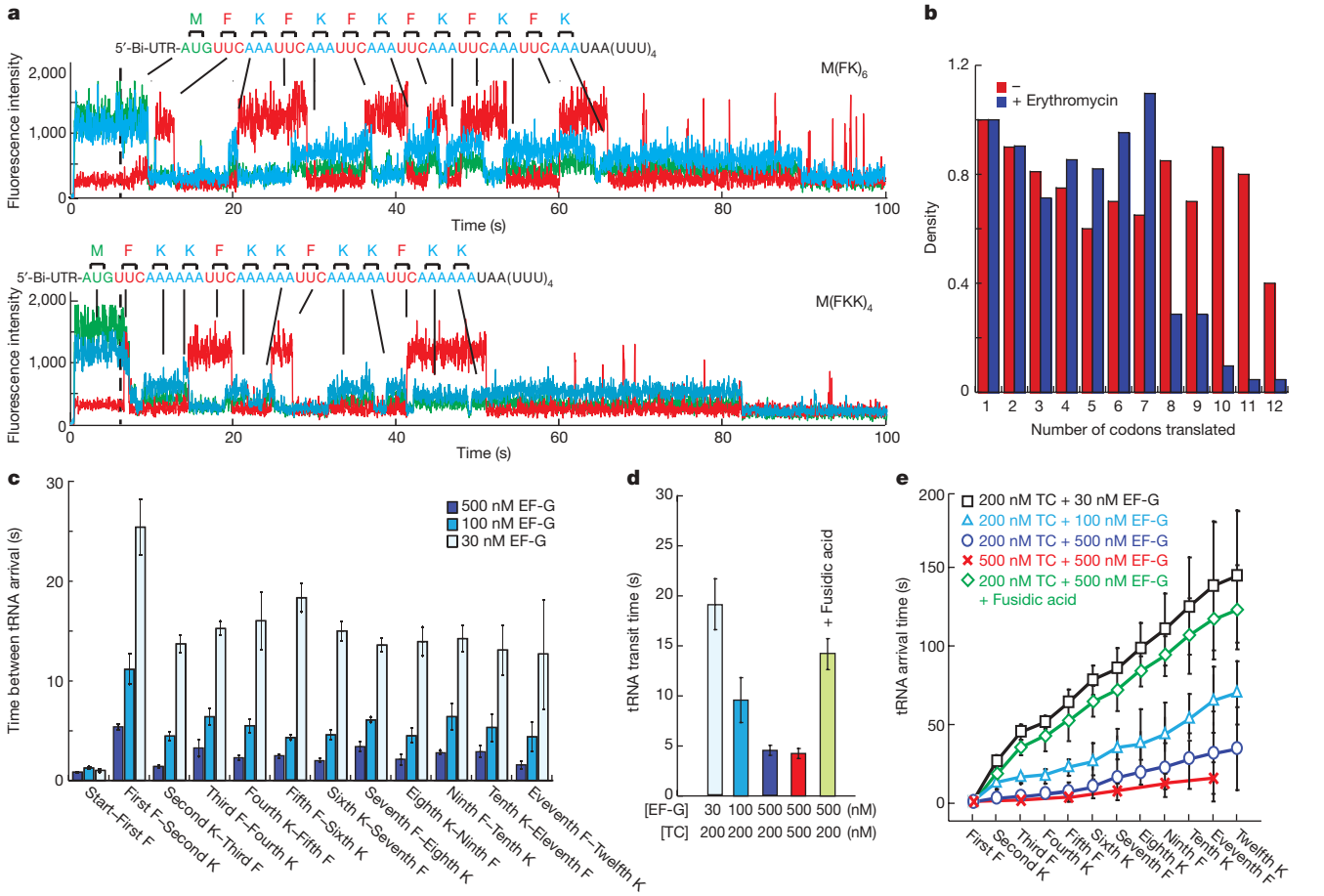

Figure 3 | Real-time translation at near-physiological concentrations. **a**, Two heteropolymeric mRNAs encoding 13 amino acids were used: $M(FK)_6$ and $M(FKK)_4$. Translation was observed in the presence of 200 nM Phe-(Cy5)$tRNA^{Phe}$, 200 nM Lys-(Cy2)$tRNA^{Lys}$ ternary complex and 500 nM EF-G as a series of fluorescent pulses that mirror the mRNA sequence. A long Cy2 pulse is observed upon arrival of the ribosome at the stop codon. Brief sampling pulses (<100 ms) of both Lys-(Cy2)$tRNA^{Lys}$ and Phe-(Cy5)$tRNA^{Phe}$ ternary complex are observed after arrival at the stop codon. **b**, Event histograms for translation of $M(FK)_6$ showing translation out to 12 elongation codons (red, $n = 381$). In the presence of 1 μM erythromycin, translation (blue, $n = 201$) is stalled at codon 8 of the mRNA. **c**, Analysis of translation rates at each codon in $M(FK)_6$. Mean times between tRNA arrival events are plotted for translation in the presence of 200 nM ternary complex and 30, 100 and 500 nM EF-G. **d**, Overall tRNA transit mean times for codons 2–12 at (from left) 200 nM ternary complex (TC) and 30, 100 or 500 nM EF-G; 500 nM ternary complex and 500 nM EF-G; and 200 nM ternary complex and 500 nM EF-G in the presence of 1 μM fusidic acid. **e**, Cumulative mean translation times for each codon in $M(FK)_6$ at 200 nM ternary complex and 30, 100 or 500 nM EF-G; 500 nM ternary complex and 500 nM EF-G; and 200 nM ternary complex and 500 nM EF-G in the presence of 1 μM fusidic acid. All error bars are 95% confidence intervals from single-exponential fits.

(Fig. 3e). This first EF-G-catalysed translocation step is about two-fold slower than subsequent translocation events, at all EF-G concentrations and for all mRNAs tested (Supplementary Fig. 5). A similar trend in elongation rate was previously observed by following the global conformation of single translating ribosomes[28]. Codons after position 3 are all translated with similar rates in $M(FK)_6$ until the long stall at the final stop codon. Slight differences in overall translation rates are observed for distinct mRNA sequences, with MF_{12} translated most slowly and $M(FKK)_4$ most rapidly (Supplementary Fig. 5). The hydrophobic character of the poly(phe) peptide may inhibit translation of the MF_{12} mRNA.

To define the mechanism linking tRNA arrival at the A site and release from the E site, we used these signals to measure the real-time tRNA occupancy of the ribosome during translation. Although at least two tRNA molecules must occupy the ribosome during peptide-bond formation[2–6], the ribosome contains three tRNA-binding sites (A, P and E), and stable tRNA occupancy in the E site after translocation would cause accumulation of three tRNA molecules on the ribosome. The arrival of tRNA in the A site may signal tRNA departure from the E site, or dissociation from the E site may occur spontaneously upon translocation. In our single-molecule traces, overlapping fluorescence pulses denote multiple tRNA molecules simultaneously bound to the ribosome, whereas appearance and departure of fluorescence indicates tRNA arrival and dissociation (Fig. 1b). During translation of the $M(FK)_6$, at 200 nM Phe-(Cy5)$tRNA^{Phe}$ and Lys-(Cy2)$tRNA^{Lys}$ ternary complex and 500 nM EF-G, most (82.2%) consecutive Cy5 and Cy2 pulses are overlapping, which indicates that two tRNA molecules occupy the ribosome simultaneously during translation.

Dynamic tRNA occupancy during translation. To determine the real-time occupancy of the ribosome at each codon, we post-synchronized 381 traces according to the arrival of aminoacylated tRNA at each codon (Fig. 5a). In this formulation, two-dimensional colour plots reveal the time-dependent tRNA occupancy of hundreds of single ribosomes during each elongation cycle along the mRNA.

This analysis shows that EF-G driven translocation controls the number of tRNA molecules on the ribosome. At 30 nM EF-G, the two-tRNA state lasts approximately 6.3 s at each codon, consistent with the estimated time for translocation. Increasing the concentrations of EF-G to 500 nM shortens the lifetime of the two-tRNA bound state of the ribosome from 6.3 s to 1.5 s (Fig. 5b). These trends are observed at different codons and for distinct mRNA sequences (Supplementary Fig. 6), confirming the generality of the conclusions. The two-tRNA state is not followed by a three-tRNA state; even at high concentrations of both EF-G and ternary complex, ribosomes occupied by three tRNA molecules are almost never observed (1.7%),

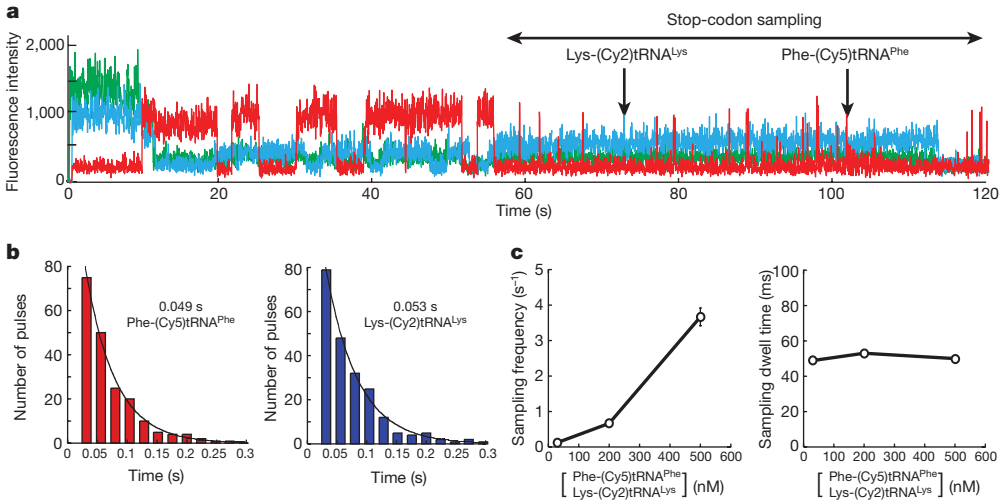

Figure 4 | A-site sampling on ribosomes stalled at the stop codon. **a**, Fast sampling events at the stop codon position of the $M(FK)_6$ template were observed in the presence of 200 nM Phe-(Cy5)tRNA^{Phe}, 200 nM Lys-(Cy2)tRNA^{Lys} ternary complex and 500 nM EF-G. **b**, Dwell-time histograms of individual sampling pulses of Phe-(Cy5)tRNA^{Phe} (left) and Lys-(Cy2)tRNA^{Lys} (right). Both histograms are well approximated by a single exponential fit. **c**, Mean frequency of fast sampling increased linearly with ternary complex concentration (left), whereas mean sampling dwell time did not depend on ternary complex concentration (right). Error bars are 95% confidence intervals from single-exponential fits.

which would be consistent with decreased E-site affinity upon A-site tRNA arrival. However, departure of E-site tRNA is not linked to arrival of the next tRNA at the A site in our experiments, as correlation analysis shows no connection between E-site tRNA departure events and A-site arrivals ($r = 0.04$). Instead, these results suggest that EF-G binding and subsequent GTP hydrolysis drive the tRNA from the A/P, P/E hybrid states to the P and E sites, at which point the E-site tRNA rapidly dissociates. Consistent with this model, fusidic-acid-stalled EF-G (GDP) in the A site inhibits arrival of the next tRNA, and inhibits each round of elongation, but does not affect the rate of tRNA dissociation from the E site (Fig. 5b).

The results presented here demonstrate that translation can be observed in real time using single ribosomes immobilized in ZMWs. The application of ZMWs to the observation of translating ribosomes allows the sensitivity and precision of single-molecule measurements at near physiological micromolar concentrations of both tRNA and protein factors (Supplementary Fig. 7). By using specifically dye-labelled tRNAs, long-lived binding events to mRNA-programmed ribosomes are readily observed and distinguished from transient sampling. The sequence of tRNA-binding events reveals the encoding mRNA sequence. Full translation requires the presence of both EF-G and the appropriate ternary complexes. Ribosome-directed antibiotics interfere with translation as predicted by their mechanism of action: fusidic acid blocks release of EF-G from the ribosome, slowing elongation, whereas erythromycin blocks elongation beyond seven amino acids. The dynamics of tRNA-binding events at each codon revealed slow initiation and long pauses upon encountering the stop codon; sampling of ternary complex at the stop codon of stalled ribosomes is observed. Translation at micromolar concentrations of factors and ligands is efficient and rapid, avoiding limitations of dye photobleaching, and allows correlation of bimolecular binding events on single ribosomes.

The mechanism by which tRNAs transit through the ribosome during decoding, peptide-bond formation and translocation was explored using our approach. Various models for the interplay of the A and E sites have been proposed. Recent dynamic and structural studies suggest that EF-G interaction within the A site may control the conformation of the E site[20]. The ability to probe tRNA dynamics on the ribosome at high ternary complex and factors concentrations in ZMWs allowed us to determine the time-dependent composition of the ribosome at each codon during translation. These results show unambiguously that tRNA release from the E site is rapid once translocation has occurred and is uncorrelated with the arrival of the next tRNA. This is consistent with a model of transient E-site occupancy after translocation[21,22].

Three tRNA molecules are rarely observed on translating ribosomes, and only at high micromolar concentrations of ternary complex, where arrival of the third tRNA molecule in the A site is rapid.

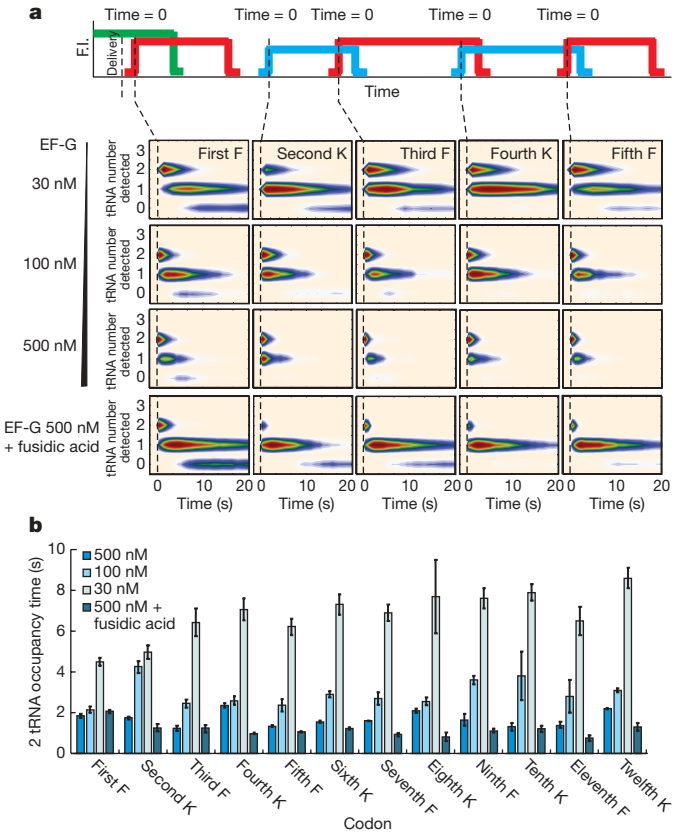

Figure 5 | Monitoring the dynamic tRNA occupancy of translating ribosomes. **a**, Post-synchronization plots for time-resolved tRNA occupancy at codons 2–6 during translation of $M(FK)_6$. Two-dimensional histograms are post-synchronized in time with respect to each tRNA transit event (First F to fifth F; F, Phe-tRNA^{Phe}; K, Lys-tRNA^{Lys}) at 500, 100 and 30 nM EF-G, and at 500 nM EF-G in the presence of fusidic acid. **b**, tRNA occupancy mean time at 500, 100 and 30 nM EF-G, and at 500 nM EF-G in the presence of fusidic acid. Error bars are 95% confidence intervals from single-exponential fits.

These data agree with dynamic investigations of the E site that show coupling of E-site opening, in particular the L1 stalk[23–25], with translocation and E-site occupancy. Rapid dissociation of the E-site tRNA upon translocation is also consistent with the fast rates required for efficient elongation. Occupancy by three tRNA molecules occurs when a slow E-site dissociation event is coincident with rapid tRNA arrival in the A site (Supplementary Fig. 7). Slow E-site dissociation delays subsequent rounds of elongation, and may be important in rare translational events, such as frameshifting[26].

Future perspectives

The real-time system outlined here has broad application to the study of translation. The dynamic events underlying translational fidelity and ribosomal movement are probed directly at each codon during translation, allowing rare translational events to be uncovered. Time-resolved analysis of compositional changes in the ribosome can be extended to initiation, elongation and release-factor binding and can be merged with FRET signals to correlate ligand binding and ribosomal conformational changes. Eukaryotic translational systems can be readily substituted to probe the dynamics of translational control and regulation. This approach allows the direct detection of mRNA coding sequence, and may allow the observation of translational events involved in the regulation of protein synthesis, such as frameshifting.

METHODS SUMMARY

Sample preparation. *Escherichia coli* ribosomal subunits and factors were prepared and purified as described[12,13]. $tRNA^{fMet}$, $tRNA^{Phe}$ and $tRNA^{Lys}$ were labelled with fluorescent dyes at their elbow positions (U8 or U47), purified and aminoacylated using previously described approaches[12,13]. Ribosome initiation complexes were assembled by combining 0.5-μM 30S subunits pre-incubated with stoichiometric S1, 0.5-μM 50S subunits, 5 μM 5′-biotinyated mRNA, 1 μM fMet-(Cy3)$tRNA^{fMet}$, 2 μM IF2 and 4 mM GTP in a polymix buffer (50 mM Tris-acetate (pH 7.5), 100 mM potassium chloride, 5 mM ammonium acetate, 0.5 mM calcium acetate, 5 mM magnesium acetate, 0.5 mM EDTA, 5 mM putrescine-HCl and 1 mM spermidine) and incubating at 37 °C for 5 min.
ZMW assay. The ZMW surface was derivatized with 1 μM neutravidin for 2 min and rinsed with the polymix buffer to remove unbound neutravidin. After rinsing, ribosome initiation complexes (diluted tenfold in polymix buffer containing 2 μM IF2 and 4 mM GTP) were delivered to the ZMW surface and incubated for 5 min at room temperature, after which the surface was rinsed with polymix buffer containing 2 μM IF2 and 4 mM GTP, as well as an oxygen scavenging system[27] (250 nM protocatechuate dioxygenase, 2.5 mM PCA (3,4-dihydroxybenzoic acid) and 1 mM Trolox). Real-time delivery solutions were prepared in polymix buffer and contained 2 μM IF2, 4 mM GTP, 30–500 nM EF-G and 30–500 nM ternary complex (one or more of the following: Phe-(Cy5)$tRNA^{Phe}$, Lys-(Cy2)$tRNA^{Lys}$ or Lys-$tRNA^{Lys}$, pre-assembled with 15 μM EF-Tu and 4 mM GTP), as well as the protocatechuate dioxygenase oxygen scavenging system.

Full Methods and any associated references are available in the online version of the paper at www.nature.com/nature.

Received 22 January 2010; accepted 18 February 2010.

1. Green, R. & Noller, H. F. Ribosomes and translation. *Annu. Rev. Biochem.* **66,** 679–716 (1997).
2. Moazed, D. & Noller, H. F. Intermediate states in the movement of transfer RNA in the ribosome. *Nature* **342,** 142–148 (1989).
3. Hausner, T. P., Geigenmüller, U. & Nierhaus, K. H. The allosteric three-site model for the ribosomal elongation cycle. New insights into the inhibition mechanism of aminoglycosides, thiostrepton, and viomycin. *J. Biol. Chem.* **263,** 13103–13111 (1988).
4. Rodnina, M. W. & Wintermeyer, W. Fidelity of aminoacyl-tRNA selection on the ribosome: kinetic and structural mechanisms. *Annu. Rev. Biochem.* **70,** 415–435 (2001).
5. Agirrezabala, X. *et al.* Visualization of the hybrid state of tRNA binding promoted by spontaneous racheting of the ribosome. *Mol. Cell* **32,** 190–197 (2008).
6. Marshall, R. A., Aitken, C. E., Dorywalska, M. & Puglisi, J. D. Translation at the single-molecule level. *Annu. Rev. Biochem.* **77,** 177–203 (2008).
7. Levene, M. J. *et al.* Zero-mode waveguides for single-molecule analysis at high concentrations. *Science* **299,** 682–686 (2003).
8. Foquet, M. *et al.* Improved fabrication of zero-mode waveguides for single-molecule detection. *J. Appl. Phys.* **103,** 034301 (2008).
9. Korlach, J. *et al.* Selective aluminum passivation for targeted immobilization of single DNA polymerase molecules in zero-mode waveguide nanostructures. *Proc. Natl Acad. Sci. USA* **105,** 1176–1181 (2008).
10. Lundquist, P. M. *et al.* Parallel confocal detection of single molecules in real time. *Opt. Lett.* **33,** 1026–1028 (2008).
11. Eid, J. *et al.* Real-time DNA sequencing from single polymerase molecules. *Science* **323,** 133–138 (2009).
12. Blanchard, S. C., Gonzalez, R. L. Jr, Kim, H. D., Chu, S. & Puglisi, J. D. tRNA selection and kinetic proofreading in translation. *Nature Struct. Mol. Biol.* **11,** 1008–1014 (2004).
13. Blanchard, S. C., Kim, H. D., Gonzalez, R. L. Jr, Puglisi, J. D. & Chu, S. tRNA dynamics on the ribosome during translation. *Proc. Natl Acad. Sci. USA* **101,** 12893–12898 (2004).
14. Chan, V., Graves, D. J. & McKenzie, S. E. The biophysics of DNA hybridization with immobilized oligonucleotide probes. *Biophys. J.* **69,** 2243–2255 (1995).
15. Schlunzen, F. *et al.* Structural basis for the interaction of antibiotics with the peptidyl transferase centre in eubacteria. *Nature* **413,** 814–821 (2001).
16. Tenson, T., Lovmar, M. & Ehrenberg, M. The mechanism of action of macrolides, lincosamides and streptogramin B reveals the nascent peptide exit path in the ribosome. *J. Mol. Biol.* **330,** 1005–1014 (2003).
17. Bodley, J. W. & Godtfredsen, W. O. Studies on translocation. XI. Structure-function relationships of the fusidane-type antibiotics. *Biochem. Biophys. Res. Commun.* **46,** 871–877 (1972).
18. Underwood, K. A., Swartz, J. R. & Puglisi, J. D. Quantitative polysome analysis identifies limitations in bacterial cell-free protein synthesis. *Biotechnol. Bioeng.* **91,** 425–435 (2005).
19. Marshall, R. A., Aitken, C. E. & Puglisi, J. D. GTP hydrolysis by IF2 guides progression of the ribosome into elongation. *Mol. Cell* **35,** 37–47 (2009).
20. Gao, Y. G. *et al.* The structure of the ribosome with elongation factor G trapped in the posttranslocational state. *Science* **326,** 694–699 (2009).
21. Lill, R. & Wintermeyer, W. Destabilization of codon-anticodon interaction in the ribosomal exit site. *J. Mol. Biol.* **196,** 137–148 (1987).
22. Semenkov, Y. P., Rodnina, M. V. & Wintermeyer, W. The ''allosteric three-site model'' of elongation cannot be confirmed in a well-defined ribosome system from *Escherichia coli*. *Proc. Natl Acad. Sci. USA* **93,** 12183–12188 (1996).
23. Cornish, P. V. *et al.* Following movement of the L1 stalk between three functional states in single ribosomes. *Proc. Natl Acad. Sci. USA* **106,** 2571–2576 (2009).
24. Fei, J., Kosuri, P., MacDougall, D. D. & Gonzalez, R. L. Jr. Coupling of ribosomal L1 stalk and tRNA dynamics during translation elongation. *Mol. Cell* **30,** 348–359 (2008).
25. Fei, J. *et al.* Allosteric collaboration between elongation factor G and the ribosomal L1 stalk directs tRNA movements during translation. *Proc. Natl Acad. Sci. USA* **106,** 15702–15707 (2009).
26. Sanders, C. L. & Curran, J. F. Genetic analysis of the E site during RF2 programmed frameshifting. *RNA* **13,** 1483–1491 (2007).
27. Aitken, C. E., Marshall, R. A. & Puglisi, J. D. An oxygen scavenging system for improvement of dye stability in single-molecule fluorescence experiments. *Biophys. J.* **94,** 1826–1835 (2008).
28. Aitken, C. E. & Puglisi, J. D. Following the intersubunit conformation of the ribosome during translation in real time. *Nat. Struct. Mol. Biol.* (in the press).

Supplementary Information is linked to the online version of the paper at www.nature.com/nature.

Acknowledgements This work was supported by National Institutes of Health grant GM51266 (to J.D.P.). We thank T. Funatsu, A. Tsai and A. Petrov for encouragement and discussions. We thank J. Gray for performing ellipsometry experiments.

Author Contributions S.U. performed all experiments and data analysis. S.U., C.E.A. and J.D.P. discussed results and wrote the manuscript. S.W.T., J.K. and B.A.F. provided technical expertise with instrumentation and data processing.

Author Information Reprints and permissions information is available at www.nature.com/reprints. The authors declare competing financial interests: details accompany the full-text HTML version of the paper at www.nature.com/nature. Correspondence and requests for materials should be addressed to J.D.P. (puglisi@stanford.edu).

METHODS

Instrumentation. Instrumentation[10] and chips containing 3,000 individual ZMWs[8] were used and prepared as described previously[11]. Specific immobilization of ribosome complexes in ZMWs was achieved by surface passivation using polyphosphonate with biotin–PEG–silane[9]. ZMW diameters were in the range 120–135 nm. Cy2, Cy3 and Cy5 fluorescence was detected upon simultaneous excitation at 488, 532 and 642 nm. Each laser power for three excitations was 0.5 $\mu W\,\mu m^{-2}$ for all three colour experiments, but 2.5 $\mu W\,\mu m^{-2}$ for two colour experiments (Fig. 2a). Each dye lifetime was 17.3 s for Phe-(Cy5)$tRNA^{fMet}$ in the P site, 22.5 s for fMet-(Cy3)$tRNA^{fMet}$ in the P site and 16.5 s for fMet-(Cy2)$tRNA^{fMet}$ in the P site.

Data collection and analysis. Data were collected on a highly parallel confocal fluorescence detection instrument, using prism-based dispersion optics and an electron-multiplying charge-coupled device camera[10]. Fluorescence traces were recorded at a rate of 30 frames per second for 3 min, with the exception experiments using MFF, MFKF mRNAs and those at 30 nM EF-G for $M(FK)_6$ mRNA, which were recorded at a rate of 100 frames per second for 5 min. Using custom software written in Matlab (MathWorks), fluorescence traces that displayed Cy3 fluorescence corresponding to an fMet-(Cy3)$tRNA^{fMet}$ molecule and co-localized with the arrival of labelled ternary complex upon delivery were analysed to extract individual tRNA transit times, time between tRNA arrivals and tRNA occupancy within single ribosomes. Data from individual molecules ($n > 200$ molecules for all experiments) were accumulated into statistical distributions to extract mean estimates for the above-described values.